RSC Advances

PAPER

View Article Online
View Journal | View Issue

Cite this: *RSC Adv.*, 2020, **10**, 11074

The influence of nanocarrier architectures on antitumor efficacy of docetaxel nanoparticles†

Zhengqi Dong,[a] Xiangtao Wang,[a] Shuang Zhao,[a] Hanhong Qiu,[a] Meihua Han,[a] Jingguo Li,[b] Ning Zhao,[c] Rui Wang[d] and Yifei Guo *[a]

Received 14th February 2020
Accepted 4th March 2020

DOI: 10.1039/d0ra01421d

rsc.li/rsc-advances

To study the structural influence, hybrid amphiphilic copolymer ($G2C_{18}$) and linear amphiphilic copolymer ($PEG_{45}C_{18}$) were utilized to prepare docetaxel (DTX)-loaded nanoparticles through an antisolvent precipitation method. The different architectures of the hydrophilic portion affected the particle sizes significantly, and then induced the different antitumor activity. Compared with DTX/$PEG_{45}C_{18}$ nanoparticles, the antitumor efficacy of DTX/$G2C_{18}$ nanoparticles was significantly enhanced, the IC_{50} value was 2.1-fold lower *in vitro*, and the inhibition rate was 1.3-fold higher *in vivo*. These results suggested that the antitumor activity was significantly affected by the architecture of the nanocarriers, and should be considered when nanocarriers are designed.

1. Introduction

Nanoscale drug delivery systems (NDDS), especially the drug-loaded nanoparticles, have been extensively researched in an attempt to improve the antitumor efficacy of hydrophobic antitumor drugs in the field of cancer therapy.[1–3] NDDS present better antitumor activity than free drugs due to the long circulation *in vivo* and high accumulation in tumor tissue.[4,5] To construct an NDDS, amphiphilic copolymers are utilized as the nanocarriers in general.[6,7] However, it is found that NDDS can be cleared easily by the reticuloendothelial system (RES), which is an obstacle to preparing effective NDDS.[8,9] To overcome this drawback, NDDS are decorated with poly(ethylene glycol) (PEG) or oligoethyleneglycol (OEG) based on their stealth properties.[10,11]

To develop effective NDDS and achieve excellent antitumor activities, it is crucial to understand the physicochemical properties of NDDS,[12,13] for example particle size,[14,15] surface charge,[16,17] morphology of drug-loaded nanoparticles,[18,19] and the preparation process.[20,21] For the physicochemical properties, it is reported that the particle size of nanoparticles plays an important role in drug delivery systems,[22,23] and influences stability, cellular internalization, tumor accumulation, biodistribution, clearance from plasma, and excretion from blood.[24] Several factors can affect particle size, including composition and molecular weight of nanocarriers,[25,26] hydrophilic/hydrophobic ratio,[27] preparation process.[28,29] When new nanocarriers are designed, several principles should be considered.[30,31] It is found that the branched structure of nanocarriers could affect the antitumor efficacy,[32] because the morphology of drug-loaded nanoparticles is related with the architecture of nanocarriers.[33]

In this study, the linear amphiphilic $PEG_{45}C_{18}$ and branched amphiphilic $G2C_{18}$ were selected as the model carriers to prepare docetaxel (DTX)-loaded nanoparticles. These two nanocarriers presented the similar composition and hydrophobic section, but the architecture of hydrophilic section was different. These two DTX-loaded nanoparticles were prepared *via* antisolvent precipitation method, and their physicochemical properties were evaluated. Furthermore, the antitumor efficacy of these two DTX-loaded nanoparticles were investigated using 4T1 tumor-bearing mice.

2. Results and discussion

DTX-loaded nanoparticles

Amphiphilic hybrid copolymer $G2C_{18}$ and linear copolymer $PEG_{45}C_{18}$ were utilized to prepare docetaxel-loaded nanoparticles (DTX/$G2C_{18}$ nanoparticles, and DTX/$PEG_{45}C_{18}$ nanoparticles) *via* antisolvent precipitation method assisted with ultrasonication (Fig. 1). According to the results of HPLC analysis, the drug-loading content (DLC) of DTX/$G2C_{18}$ nanoparticles and DTX/$PEG_{45}C_{18}$ nanoparticles was (72.2 ± 0.6)% and (67.7 ± 1.9)%, respectively (ESI, Table S1†), which were slightly lower than the theoretical value of 80% due to the dialysis and homogenization process.

[a]*Institute of Medicinal Plant Development, Chinese Academy of Medical Sciences & Peking Union Medical College, Beijing 100193, P. R. China. E-mail: ffguo@163.com; Fax: +86-10-57833266; Tel: +86-10-57833266*

[b]*Zhengzhou University People's Hospital, No. 7, Weiwu Road, Zhengzhou, 450003, PR China*

[c]*Department of Pharmacy, Xiyuan Hospital, China Academy of Chinese Medical Sciences, No. 1, Xiyuancaochang, Haidian District, Beijing 100091, China*

[d]*School of Pharmacy, Heilongjiang University of Chinese Medicine, No. 24, Heping Road, Xiangfang District, Harbin 150040, China*

† Electronic supplementary information (ESI) available. See DOI: 10.1039/d0ra01421d

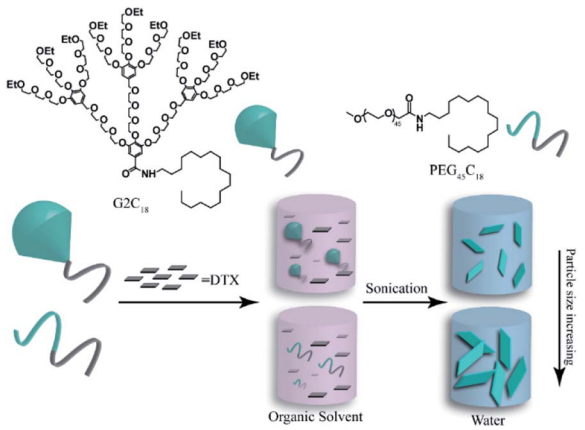

Fig. 1 Structure of amphiphilic copolymers and the preparation process of DTX-loaded nanoparticles.

Characterization

These two DTX nanoparticles exhibited the similar distribution property (PDI = 0.12–0.14) and zeta potential value (21.4–29.1 mV) (ESI, Table S1†). The particle size distribution curves of these two nanoparticles are shown in Fig. 2a and c, it was clear that both of them showed the uniform dispersion and narrow particle size distribution. On the contrary, these two DTX nanoparticles presented different particle size, the mean hydrodynamic diameter was approximately 255.6 and 396.8 nm for DTX/G2C_{18} nanoparticles and DTX/PEG$_{45}C_{18}$ nanoparticles respectively. The different particle size might be affected by the steric hindrance of nanocarriers. During the assembly process, steric hindrance could hamper tiny nanocrystals to form large nanoaggregates. Compared with liner nanocarriers PEG$_{45}C_{18}$, hybrid nanocarriers G2C_{18} presented stronger steric hindrance obviously, because hydrophilic OEG dendron exhibited the branched architecture. After G2C_{18} interacting with DTX and forming tiny nanoparticles, the outer hydrophilic OEG dendron would act as the protective layer to prevent DTX nanoparticles growth furthermore, therefore, the DTX nanoparticles exhibited the relative small particle sizes.

The morphology of DTX/G2C_{18} nanoparticles and DTX/PEG$_{45}C_{18}$ nanoparticles was observed by scanning electron microscopy (SEM), the images are shown in Fig. 2b and d. Both of DTX nanoparticles were uniformly dispersed as regular nanosheets. From SEM images, it could be seen that the particle size of DTX/PEG$_{45}C_{18}$ nanoparticles was larger than DTX/G2C_{18} nanoparticles, which was consistent with dynamic light scanning results.

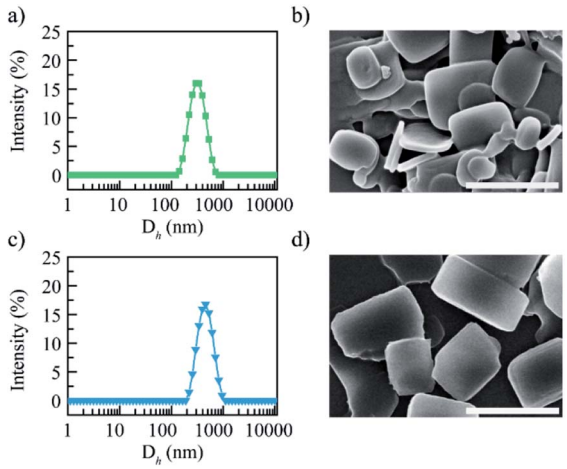

Fig. 2 Particle size distribution curves and SEM images of DTX nanoparticles. Particle size distribution curves of DTX/G2C_{18} nanoparticles (a), DTX/PEG$_{45}C_{18}$ nanoparticles (c), SEM images of DTX/G2C_{18} nanoparticles (b), DTX/PEG$_{45}C_{18}$ nanoparticles (d). Scale bar: 100 nm (b), 500 nm (d).

Stability

The possibility of intravenous administration of nanoparticles is affected by their stability and erythrocyte toxicity. DTX/G2C_{18} nanoparticles and DTX/PEG$_{45}C_{18}$ nanoparticles were stored at 4 °C, the particle size of these samples was about 271.8 ± 11.8 nm and 445.8 ± 8.5 nm after 7 days, respectively (ESI, Fig. S1a†). Comparing with the initial value, the particle size increased slightly, this may be caused by Ostwald ripening.[34] In the following 3 weeks, the particles sizes of these two nanoparticles presented no significant change.

Then, the media stability was evaluated by mixing DTX nanoparticles with different media, including PBS, 5% glucose solution, and normal saline solution. Unfortunately, after mixing DTX nanoparticle solutions with PBS or normal saline solution, turbidity or precipitate was shown, the particle sizes were increased over 1 μm, revealing DTX nanoparticles were unstable in these media. On the contrary, after 6 h incubation in 5% glucose solution, there was no significant change was shown, and the particle size of two DTX nanoparticles were maintained comparing with their initial size (ESI, Fig. S1b†). The similar results were shown in plasma after incubating 6 h (ESI, Fig. S1c†). These results proved these two DTX nanoparticles could be stable in 5% glucose solution and plasma, suggesting they exhibited the potential application *via* intravenous administration.

Drug release profile

DTX/G2C_{18} nanoparticles and DTX/PEG$_{45}C_{18}$ nanoparticles were released at 37 °C in PBS (pH 7.4) containing SDS (0.5%, wt%), DTX solution was used as control (ESI, Fig. S2†). DTX solution presented the high cumulative release rate of approximately 82.6% within 24 h, and exhibiting the significant burst release, over 70% DTX was released at the initial 4 h. Under the same condition, the release process of DTX/G2C_{18} nanoparticles and DTX/PEG$_{45}C_{18}$ nanoparticles was slow and steady, no initial burst release was shown. The entire release process of these two DTX nanoparticles were formed by two phase: it was almost zero-order release before 4 day with the cumulative release rate of approximately 60%, then the release became slow, and the cumulative release rate increased by only 30% in the following 4 day. Between these two DTX nanoparticles, they presented the similar release process, and no significant difference was shown. While, comparing with DTX

solution, nanoparticles existed obvious sustained release profile. This phenomenon was consisted with the previous results,[35] and could be explained by the structure of DTX nanoparticles, the hydrophilic shell of the DTX nanoparticles hindered the diffusion of DTX from the inner core of nanoparticles to the release medium.

In vitro cytotoxicity

$DTX/G2C_{18}$ nanoparticles and $DTX/PEG_{45}C_{18}$ nanoparticles were incubated in 4% erythrocyte suspension at 37 °C for 4 h. The hemolysis percentage of both DTX nanoparticles were less than 5% at the concentration of 0.06–1 mg mL^{-1}. It could be seen that both DTX nanoparticles exhibited good red cell biocompatibility, and were suitable for intravenous injection.

The cytotoxicity of DTX nanoparticles towards 4T1 cells was determined *via* a MTT method. The concentration ranged from 0.01 to 100 μg mL^{-1} (DTX equivalent concentration, Fig. 3a). Amphiphilic nanocarriers showed no significant cytotoxicity towards 4T1 cells over the whole test concentration. After incubation 48 h, the inhibitory effects of all DTX samples were concentration-dependent. Compared with free DTX, DTX nanoparticles had higher cytotoxicity against 4T1 cells at the same concentration, IC_{50} value was 1.7 and 3.6 μg mL^{-1} for $DTX/G2C_{18}$ nanoparticles and $DTX/PEG_{45}C_{18}$ nanoparticles separately, 5.6 μg mL^{-1} for free DTX. Both the DTX nanoparticles exhibited the significant difference ($p < 0.05$, *vs.* free DTX). These results showed that more DTX in nanoparticles were transferred into tumor cells, due to nanoparticles entered into cell *via* the facilitated endocytosis transport, and free DTX cross cell membrane through the passive diffusion. These results proved that the activity of DTX nanoparticles was greater than that of free drugs, because the nanoparticles are easily ingested by endocytosis pathway, which effectively avoid the effect of multi-drug resistance induced by free drugs.[36] Importantly, the antitumor effect of $DTX/G2C_{18}$ nanoparticles is higher than that of $DTX/PEG_{45}C_{18}$ nanoparticles *in vitro*. This phenomenon could be attributed to the influence of particle size, those nanoparticles with small diameter could be transferred into tumor cells more easily due to the low energy consumption,[37] therefore, $DTX/G2C_{18}$ nanoparticles showed higher cytotoxicity towards 4T1 cells.

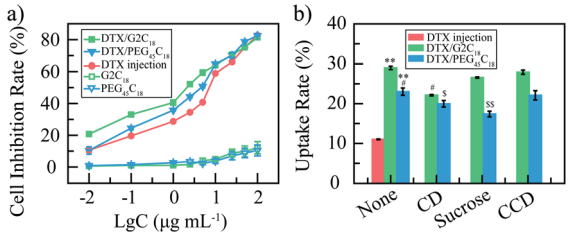

Fig. 3 The cytotoxicity and cellular uptake of DTX nanoparticles. The cytotoxicity of $DTX/G2C_{18}$ nanoparticles and $DTX/PEG_{45}C_{18}$ nanoparticles towards 4T1 cells (a), cellular uptake (b) ($n = 5$). $^{**}p < 0.01$ *vs.* DTX solution, $^{\#}p < 0.05$ *vs.* $DTX/G2C_{18}$ nanoparticles, $^{\$}p < 0.05$, $^{\$\$}p < 0.01$ *vs.* $DTX/PEG_{45}C_{18}$ nanoparticles.

Cellular uptake

To investigate the cellular uptake mechanism, DTX nanoparticles were co-incubated with 4T1 cells, and the uptake ratio was calculated based on the actual DTX concentration in these cells (Fig. 3b). The cell uptake rate of DTX nanoparticles group was significantly higher than that of DTX solution group (29.9%, 23.4% *vs.* 11.0%, $p < 0.01$), which was consisted with the results of MTT assay. Furthermore, the uptake rate of $DTX/G2C_{18}$ nanoparticles was higher than that of $DTX/PEG_{45}C_{18}$ nanoparticles (29.9% *vs.* 23.4%, $p < 0.05$), due to the different particle size. To prove the endocytosis pathway during the internalization process, 4T1 cells were cultured with different endocytosis inhibitors, including caveolae-mediated endocytosis, clathrin-mediated endocytosis, and macropincytosis-dependent endocytosis. After incubation with endocytosis inhibitors such as sucrose, hydroxypropyl-CD, and cytochalasin D, it was found that the cell uptake of $DTX/G2C_{18}$ nanoparticles was affected by hydroxypropyl-CD significantly ($p < 0.05$). The endocytosis mechanism for $DTX/G2C_{18}$ nanoparticles was caveolae-mediated pathway, which could be attributed to the sheet-like morphology.[35] For $DTX/PEG_{45}C_{18}$ nanoparticles, the cellular uptake rates were affected by hydroxypropyl-CD ($p < 0.05$) and surcose significantly ($p < 0.01$), indicating the endocytosis process were caveolae-mediated pathway and clathrin-mediated pathway. These results suggested that the endocytosis pathway were influenced by morphology and particle size of drug-loaded nanoparticles.[38,39]

Animal experiments

The antitumor activities of $DTX/G2C_{18}$ nanoparticles and $DTX/PEG_{45}C_{18}$ nanoparticles were studied in 4T1 tumor-bearing mice, 5% glucose solution and DTX injection were used as control. The tumor-bearing mice were randomly divided into 4 groups ($n = 8$): 5% glucose solution group (blank control), DTX injection group (positive control), $DTX/G2C_{18}$ nanoparticles group and $DTX/PEG_{45}C_{18}$ nanoparticles group (test groups). The dose of 10 mg kg^{-1} (DTX equivalent concentration) was given every two days for 6 times. The changes of tumor volume of mice in each group were monitored, as shown in Fig. 4a. It can be seen that the tumor volume increased the most in glucose solution group, followed by DTX injection group. The tumor volume growth in these two DTX nanoparticles groups were significantly lower than that in the glucose solution group and PTX injection group. Compared with the commercial DTX injection, DTX nanoparticles achieved better inhibitory effect on tumor growth, especially $DTX/G2C_{18}$ nanoparticles group. The more important reason may be that the nanoparticles owned suitable particle size, which could be passively targeted to the tumor tissue through the EPR effect and absorbed by tumor cells with higher uptake efficiency, so as to achieve a stronger antitumor effect.

At the end of experiment, the mice were killed, the tumor tissues were completely stripped and weighed (Fig. 4b), and the tumor inhibition rate based on the tumor weight was calculated. The tumor weights of glucose, DTX injection, $DTX/G2C_{18}$ nanoparticles, and $DTX/PEG_{45}C_{18}$ nanoparticles groups were

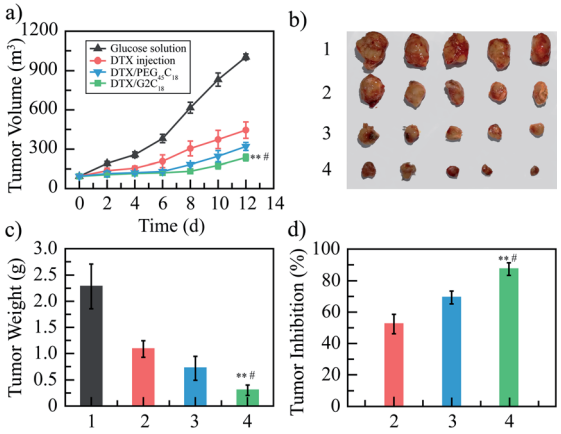

Fig. 4 Tumor growth inhibition of DTX/G2C_{18} nanoparticles and DTX/$PEG_{45}C_{18}$ nanoparticles. Tumor volume change curves (a), tumor tissue image (b), tumor weight (c), and tumor inhibition rate based on tumor tissue weight (d). 1: Glucose solution group, 2: DTX injection group, 3: DTX/$PEG_{45}C_{18}$ nanoparticle group, 4: DTX/G2C_{18} nanoparticle group ($n = 8$). $^{**}p < 0.01$ *vs.* DTX solution, $^{\#}p < 0.05$ *vs.* $PEG_{45}C_{18}$ nanoparticles.

2.28 ± 0.42, 1.09 ± 0.15, 0.30 ± 0.09, and 0.70 ± 0.22 g, respectively (Fig. 4c). The tumor inhibition rates of DTX injection, DTX/G2C_{18} nanoparticles, and DTX/$PEG_{45}C_{18}$ nanoparticles groups was 52.4%, 86.7%, and 69.3%, separately (Fig. 4d). It can be seen that the tumor inhibition rate of two DTX nanoparticles on 4T1 tumor-bearing mice was significantly higher than that of DTX injection group, and DTX/G2C_{18} nanoparticles showed better inhibitory effect on tumor growth than DTX/$PEG_{45}C_{18}$ nanoparticles, further proved that DTX/G2C_{18} nanoparticles possessed stronger antitumor activity. Both of the antitumor efficacy based on tumor growth curves and tumor weight verified DTX/G2C_{18} nanoparticles presented enhanced antitumor efficacy, because the branched architecture in the nanocarriers formed the nanoparticle with small particle size and then induced the higher endocytosis rate,[40,41] these results were in good agreement with MTT assay.

3. Conclusion

In this study, branched OEG dendron (G2) and linear PEG chain (PEG_{45}) with the similar molecular weight were conjugated with octadecylamine (C_{18}) to form the amphiphilic copolymers (G2C_{18} and $PEG_{45}C_{18}$). To study the influence of branched architecture on antitumor activity, the amphiphilic copolymers G2C_{18} and $PEG_{45}C_{18}$ were utilized as nanocarriers to prepare docetaxel-loaded nanoparticles, the antitumor effects of two DTX nanoparticles were studied *in vitro* and *in vivo*. These two DTX nanoparticles presented the similar drug-loading content of approximately 70%, the sheet-like morphology, and sustained release profiles. However, the different architecture of nanocarriers induced the different particle size of DTX nanoparticles. Compared with DTX/$PEG_{45}C_{18}$ nanoparticles, DTX/G2C_{18} nanoparticles exhibited the smaller particle size, the hydrodynamic diameter was approximately 255.6 nm, due to the strong steric hindrance of branched architecture hindered nanoparticles growth. Based on the suitable particle diameter, the antitumor activity of DTX/G2C_{18} nanoparticles was significantly enhanced, the IC_{50} value was 2.1-fold lower than that of DTX/$PEG_{45}C_{18}$ nanoparticles ($p < 0.05$) *in vitro*, and the inhibition rate was 1.3-fold higher *in vivo*. These results suggested that the antitumor activity might be related with the architecture of nanocarriers, which should be considered and optimized in the design of nanocarriers.

Ethical statement

All experimental procedures were performed according to the Guidelines and Policies for Ethical and Regulatory for Animal Experiments and approved by the Animal Ethics Committee of Peking Union Medical College (Beijing, China).

Conflicts of interest

There are no conflicts to declare.

Acknowledgements

This work is financially supported by the National Key Research and Development Project (no. 2018YFC1706700), National Major Scientific and Technological Special Project for "Significant New Drugs Development" (no. 2015ZX09501005), CAMS Innovation Fund for Medical Sciences (CIFMS, no. 2017-I2M-1-013, 2016-I2M-1-012).

Notes and references

1 Y. Xin, Q. Huang, J.-Q. Tang, X.-Y. Hou, P. Zhang, L. Z. Zhang and G. Jiang, *Cancer Lett.*, 2016, **379**, 24–31.
2 V. R. Devadasu, V. Bhardwaj and M. N. V. R. Kumar, *Chem. Rev.*, 2013, **113**, 1686–1735.
3 M. W. Tibbitt, J. E. Dahlman and R. Langer, *J. Am. Chem. Soc.*, 2016, **138**, 704–717.
4 F. Zhang, G. Zhu, O. Jacobson, Y. Liu, K. Chen, G. Yu, Q. Ni, J. Fan, Z. Yang, F. Xu, X. Fu, Z. Wang, Y. Ma, G. Niu, X. Zhao and X. Chen, *ACS Nano*, 2017, **11**, 8838–8848.
5 S. Sunoqrot, J. Bugno, D. Lantvit, J. E. Burdette and S. Hong, *J. Controlled Release*, 2014, **191**, 115–122.
6 K. Letchford and H. Burt, *Eur. J. Pharm. Biopharm.*, 2007, **65**, 259–269.
7 A. Rösler, G. W. M. Vandermeulen and H.-A. Klok, *Adv. Drug Delivery Rev.*, 2012, **64**, 270–279.
8 S.-D. Li and L. Huang, *Biochim. Biophys. Acta, Biomembr.*, 2009, **1788**, 2259–2266.
9 D. E. Owens and N. A. Peppas, *Int. J. Pharm.*, 2006, **307**, 93–102.
10 S.-D. Li and L. Huang, *J. Controlled Release*, 2010, **145**, 178–181.
11 H. Xiao, J. F. Stefanick, X. Jia, X. Jing, T. Kiziltepe, Y. Zhang and B. Bilgicer, *Chem. Commun.*, 2013, **49**, 4809–4811.
12 H. Ragelle, R. Riva, G. Vandermeulen, B. Naeye, V. Pourcelle, C. S. Le Duff, C. D'Haese, B. Nysten, K. Braeckmans, S. C. De

Smedt, C. Jérôme and V. Préat, *J. Controlled Release*, 2014, **176**, 54–63.
13 M. Durán-Lobato, L. Martín-Banderas, R. Lopes, L. M. D. Gonçalves, M. Fernández-Arévalo and A. J. Almeida, *Drug Dev. Ind. Pharm.*, 2016, **42**, 190–198.
14 D. S. Kohane, *Biotechnol. Bioeng.*, 2007, **96**, 203–209.
15 L. Tang, X. Yang, Q. Yin, K. Cai, H. Wang, I. Chaudhury, C. Yao, Q. Zhou, M. Kwon, J. A. Hartman, I. T. Dobrucki, L. W. Dobrucki, L. B. Borst, S. Lezmi, W. G. Helferich, A. L. Ferguson, T. M. Fan and J. Cheng, *Proc. Natl. Acad. Sci. U. S. A.*, 2014, **111**, 15344–15349.
16 X. Liu, H. Li, Q. Jin and J. Ji, *Small*, 2014, **10**, 4230–4242.
17 H.-X. Wang, Z.-Q. Zuo, J.-Z. Du, Y.-C. Wang, R. Sun, Z.-T. Cao, X.-D. Ye, J.-L. Wang, K. W. Leong and J. Wang, *Nano Today*, 2016, **11**, 133–144.
18 M. Caldorera-Moore, N. Guimard, L. Shi and K. Roy, *Expert Opin. Drug Delivery*, 2010, **7**, 479–495.
19 H. Wang, J. Feng, G. Liu, B. Chen, Y. Jiang and Q. Xie, *Nanomedicine*, 2016, **12**, 881–891.
20 K. Langer, S. Balthasar, V. Vogel, N. Dinauer, H. von Briesen and D. Schubert, *Int. J. Pharm.*, 2003, **257**, 169–180.
21 J. Guan, P. Cheng, S. J. Huang, J. M. Wu, Z. H. Li, X. D. You, L. M. Hao, Y. Guo, R. X. Li and H. Zhang, *Phys. Procedia*, 2011, **22**, 163–169.
22 X.-D. Zhang, D. Wu, X. Shen, J. Chen, Y.-M. Sun, P.-X. Liu and X.-J. Liang, *Biomaterials*, 2012, **33**, 6408–6419.
23 A. Sen Gupta, *Wiley Interdiscip. Rev.: Nanomed. Nanobiotechnol.*, 2016, **8**, 255–270.
24 S. A. Kulkarni and S.-S. Feng, *Pharm. Res.*, 2013, **30**, 2512–2522.
25 K. Park, J.-H. Kim, Y. S. Nam, S. Lee, H. Y. Nam, K. Kim, J. H. Park, I.-S. Kim, K. Choi, S. Y. Kim and I. C. Kwon, *J. Controlled Release*, 2007, **122**, 305–314.
26 A. Almalik, R. Donno, C. J. Cadman, F. Cellesi, P. J. Day and N. Tirelli, *J. Controlled Release*, 2013, **172**, 1142–1150.
27 Z. Cao, Q. Yu, H. Xue, G. Cheng and S. Jiang, *Angew. Chem., Int. Ed.*, 2010, **49**, 3771–3776.
28 B. Sinha, R. H. Müller and J. P. Möschwitzer, *Int. J. Pharm.*, 2013, **453**, 126–141.
29 C. Qian and D. J. McClements, *Food Hydrocolloids*, 2011, **25**, 1000–1008.
30 E. Blanco, H. Shen and M. Ferrari, *Nat. Biotechnol.*, 2015, **33**, 941–951.
31 H. S. Choi, W. Liu, F. Liu, K. Nasr, P. Misra, M. G. Bawendi and J. V. Frangioni, *Nat. Nanotechnol.*, 2010, **5**, 42–47.
32 G. M. Soliman, A. Sharma, D. Maysinger and A. Kakkar, *Chem. Commun.*, 2011, **47**, 9572–9587.
33 Y. Guo, T. Wang, H. Qiu, M. Han, Z. Dong, X. Wang and Y. Wang, *Eur. J. Pharm. Biopharm.*, 2019, **134**, 178–184.
34 S. G. Rinaldo, *Phys. Rev. E: Stat., Nonlinear, Soft Matter Phys.*, 2012, **86**, 041601.
35 Y. Guo, S. Zhao, H. Qiu, T. Wang, Y. Zhao, M. Han, Z. Dong and X. Wang, *Bioconjugate Chem.*, 2018, **29**, 1302–1311.
36 J. Kim, J. C. Sunshine and J. J. Green, *Bioconjugate Chem.*, 2014, **25**, 43–51.
37 W.-K. Oh, S. Kim, M. Choi, C. Kim, Y. S. Jeong, B.-R. Cho, J.-S. Hahn and J. Jang, *ACS Nano*, 2010, **4**, 5301–5313.
38 W. Zhang, J. Sun, Y. Liu, M. Tao, X. Ai, X. Su, C. Cai, Y. Tang, Z. Feng, X. Yan, G. Chen and Z. He, *Mol. Pharmaceutics*, 2014, **11**, 3279–3290.
39 A. M. Bannunah, D. Vllasaliu, J. Lord and S. Stolnik, *Mol. Pharmaceutics*, 2014, **11**, 4363–4373.
40 L. Tang, N. P. Gabrielson, F. M. Uckun, T. M. Fan and J. Cheng, *Mol. Pharmaceutics*, 2013, **10**, 883–892.
41 X. Sun, J. Zhang, C. Yang, Z. Huang, M. Shi, S. Pan, H. Hu, M. Qiao, D. Chen and X. Zhao, *ACS Appl. Mater. Interfaces*, 2019, **11**, 11865–11875.